Possible optical functions of the central core in lenses of trilobite eyes: spherically corrected monofocality or bifocality

Ádám Egri and Gábor Horváth*

Environmental Optics Laboratory, Department of Biological Physics, Physical Institute, Eötvös University, H-1117 Budapest, Pázmány sétány 1, Hungary
**Corresponding author: gh@arago.elte.hu*

Received June 15, 2012; accepted July 17, 2012;
posted July 24, 2012 (Doc. ID 170784); published August 29, 2012

The function of the central core in lenses of certain schizochroal-eyed trilobites is unknown. To understand the possible optical function(s) of this central core, we performed computational ray-tracing on the lens in the schizochroal compound eyes of a Silurian *Dalmanites* trilobite. We computed the intensity of light focused by the lens versus the distance from the lower lens surface along the optical axis as functions of the refractive indices n_{lu} and n_{cc} of the lower lens unit and the central core. We determined those values of n_{lu} and n_{cc} that ensure that the studied central-cored trilobite lens is monofocal, bifocal, or trifocal. The sharpness (as the measure of the correction for spherical aberration) of these focal points was quantitatively studied. We show here that one of the possible optical functions of the central core could be the correction for spherical aberration, independently of the number (1, 2, or 3) of focal points. Another possible optical function of the core could be to ensure bifocality of the lens. In this case the peripheral lens region could have a given focal length and the central lens region could possess a longer or shorter focal length, if the refractive index n_{cc} of the core is smaller or larger than the refractive index n_{lu} of the upper lens unit. Finally, trifocality of the lenses can be considered only as a theoretical option, but by no means an optically optimally functioning possibility.

OCIS codes: 330.5370, 080.3630.

1. INTRODUCTION

The cuticle of trilobites is composed of calcite embedded into an organic matrix [1]. The majority of trilobites had compound eyes, and their lenses were made of calcite too [2–6]. The first trilobites with eyes appeared about 520 million years ago in the Cambrian, and the last trilobites became extinct at the end of the Permian, about 220 million years ago. Only the lenses and adjacent cuticular regions have been preserved, and all the photoreceptors and other structures have decayed tracelessly. Three different types of eyes are known in trilobites: holochroal, schizochroal, and abathochroal [3–9].

Holochroal eyes represent the ancestral type. They had many small (diameter = 10–20 μm), closely packed calcitic lenses possessing a circular or hexagonal cross section and concavely curved outer and inner refractive surfaces. A thin calcitic cornea covered the lenses with rounded outer and inner surfaces. Calcite is a birefringent mineral breaking light into two rays, which would produce double images at different depths. There is, however, the crystallographic *c*-axis in which light travels through without being affected. In all trilobite eyes the *c*-axis of the lenses was the same as the optical axis, so that the birefringence of calcite was minimized. The holochroal eyes of certain trilobites (e.g., *Carolinites*) were adapted to relatively bright light, while others (e.g., *Pricyclopyge*) functioned at lower light levels [10,11]. Trilobites, usually with kidney-shaped holochroal eyes, adapted to dim or moderate light intensities, and persisted until the close of the Permian.

The schizochroal eyes were large, with relatively low numbers (maximum a few hundred) of lenses [3,4,7,12]. The almost biconvex schizochroal lenses were much larger (diameter = 100–350 μm) than the holochroal lenses (10–20 μm). They were separated from each other by a cuticle, and each lens had its own thin cornea [13]. The schizochroal lenses had usually two main units: the upper unit was composed of calcite, while the lower unit consisted of an organic material [14]. In the eye of the early Ordovician *Dalmanitina socialis*, for example, the upper surface of the lower lens unit was indented with a tiny dimple, whereas in the contemporaneous *Crozonaspis struvei*, the lower unit was much thicker with a wavy upper surface. The function of this wavy surface was to correct for spherical aberration of the whole lens [15–17]. The function of the lower unit itself was to reduce the internal reflections due to its intermediate refractive index ($n = 1.40$–1.53) between the indices of refraction of the calcitic upper lens unit ($n = 1.66$) and the body fluid ($n = 1.36$) below the lens [16,18].

The lower surface of the upper lens unit in *Dalmanitina socialis* had a little nipple, and it has been shown [19] that this bulge made the whole doublet lens bifocal (with two sharp focal points below the lens) so that the trilobite could see simultaneously far and near in spite of the fact that its rigid lens was not able to accommodate.

In *Phacops rana milleri* and *Eldredgeops rana rana*, the lower lens unit thinned out and vanished centrally, while an additional structure, the core, of similar appearance to the lower unit, was placed in the center of the lens [12,20]. In

some other phacopid trilobites, there was a core as well, but less highly differentiated. Schizochroal eyes derived from holochroal precursors [21,22].

Schizochroal eyes have some living counterparts, because certain larval insect eyes (known as *stemmata*) do possess rather similar features, including a separation into upper and lower lens units [23,24]. The nearest counterpart of schizochroal eyes is in the males of night-flying insects known as strepsipterans, having relatively (to the eyes) large and separated lenses. Below each lens there is a retina, on which the image is formed and sampled by many photoreceptors [25]. It is hypothesized that under each lens of schizochroal trilobite eyes was a short capsule floored by 1000 or more retinal cells [4,26,27].

The abathochroal trilobite eyes looked like tiny schizochroal eyes, with separated lenses, but there was no interlensar sclera, and the packing system was relatively irregular [28]. In the abathochroal-eyed *Neocobboldia chinlinica*, the lower lens surface had a little nipple, and it has been suggested [29] that this bulge made the lens bifocal so that it could see both near and far, even though the focal point below the bulge was not sharp, due to light diffraction. Many further details of trilobite eyes have been summarized in [22].

In principle, the core could have had some kind of mechanical (e.g., supporting) function, for instance. However, this is not too probable, because the upper lens unit, with the enigmatic core in its center, was composed of hard calcite that does not need mechanical support. Rather, the core might have had certain kinds of optical function. According to our hypothesis, these functions could be monofocality or bifocality with correction for spherical aberration. In this work we test this hypothesis by means of computational ray-tracing through a typical central-cored trilobite lens. We present here the results of our geometric optical studies and draw conclusions on the conditions under which the lens core can ensure spherically corrected monofocality or bifocality.

2. MATERIALS AND METHODS

A. Shape of Central-Cored Trilobite Lenses

The homogenous appearance of the central lens core suggests that its homogeneity has not changed [3,5,7–9, 15,22]. According to the fossil records that have no diagenetic artifacts, the position, size, and shape of this core have not changed during fossilization [12]. We studied the central-cored lens of a Silurian *Dalmanites* trilobite (Fig. 1(a)). The main longitudinal section of the lenses parallel to the optical axis originated from [15]. Using the method of least squares, we fitted the following five functions to the longitudinal sections of the refractive surfaces of the lens in the r–z coordinate system in Fig. 1(b): $f_1(r)$, outer lens surface; $f_2(r)$, inner lens surface; $f_3(r)$, interface between the upper and lower lens units; $f_4(r)$, upper surface of the central core; $f_5(r)$, lower surface of the central core, where $r = (x^2 + y^2)^{1/2}$. These five functions describe mathematically the shape of the trilobite lens investigated, the optical axis z of which coincides with its axis of rotational symmetry. We assumed that the outer lens surface contacts with seawater with a refractive index $n_w = 1.33$, and the inner lens surface contacts with body fluid with a refractive index $n_{\mathrm{bf}} = 1.36$. The refractive index of the calcite upper lens unit is $n_{\mathrm{uu}} = 1.66$. The refractive indices of the lower lens unit (n_{lu}) and the central core (n_{cc}) were variable parameters.

The mathematical expressions and the numerical values of their parameters describing the lens shape in the studied Silurian *Dalmanites* are the following (Fig. 1):

$$
\begin{aligned}
&f_1(r) = A_1 + B_1 r^2,\\
&f_2(r) = A_2 + B_2 r^2,\\
&f_3(r) = A_3 + B_3 \cos(C_3 r),\\
&f_4(r) = \begin{cases} A_4(1 - r^2/B_4^2)^{1/2} & r \le B_4 \\ 0 & \text{otherwise} \end{cases},\\
&f_5(r) = \begin{cases} A_5(1 - r^2/B_5^2)^{1/2} & r \le B_5 \\ 0 & \text{otherwise} \end{cases},\\
&A_1 = 0.572039 \cdot R, \quad B_1 = -0.425220/R, \quad A_2 = -1.065815 \cdot R,\\
&B_2 = -0.358080/R, \quad A_3 = -0.774962 \cdot R, \quad B_3 = -0.224472 \cdot R,\\
&C_3 = 3.368190/R, \quad A_4 = 0.268429 \cdot R, \quad B_4 = 0.316354 \cdot R,\\
&A_5 = -0.437346 \cdot R, \quad B_5 = B_4,
\end{aligned} \tag{1}
$$

where R is the lens radius, and $r = \sqrt{x^2 + y^2}$.

B. Computational Ray-Tracing through a Central-Cored Trilobite Lens

Using the shape of the central-cored trilobite lens described above (Fig. 1), we performed the following three-dimensional (3D) computational ray-tracing.

1. Intersection of a Refractive Surface and a Ray

Consider a refractive surface described by the function $f(x, y)$ in the 3D space, and a light ray with direction $\underline{e}_0 = (e_{0x}, e_{0y}, e_{0z})$ starting from the point $\underline{p}_0 = (p_{0x}, p_{0y}, p_{0z})$, where $\underline{e}_0$ is a unit vector (Fig. 2). The path of the ray can be written in parametric format:

$$
\begin{aligned}
&\underline{p}(t) = \underline{p}_0 + \underline{e}_0 \cdot t \rightarrow x(t) = x_0 + e_{0x} \cdot t,\\
&y(t) = y_0 + e_{0y} \cdot t, z(t) = z_0 + e_{0z} \cdot t,
\end{aligned} \tag{2}
$$

where t is the control parameter. The coordinates where the ray hits the surface $f(x, y)$ can be determined from the equation

$$
f(x_0 + e_{0x} \cdot t, y_0 + e_{0y} \cdot t) = z_0 + e_{0z} \cdot t. \tag{3}
$$

2. Refraction at the Lens Surfaces

After finding the point of intersection of the refractive surface and the investigated ray, the new direction of the refracted ray has to be computed with the use of the Snellius–DesCartes law. The unit normal vector $\underline{N}$ of refractive surface $f(x, y)$ is (Fig. 2)

$$
\begin{aligned}
&\underline{N} = \frac{\underline{e}_1 \times \underline{e}_2}{|\underline{e}_1 \times \underline{e}_2|}, \quad \text{with} \quad \underline{e}_1 = \left(1, 0, \frac{\partial f(x, y)}{\partial x}\right),\\
&\underline{e}_2 = \left(0, 1, \frac{\partial f(x, y)}{\partial y}\right).
\end{aligned} \tag{4}
$$

The unit vector of the new direction of refracted ray is

$$\underline{e}_{\text{new}} = \frac{\underline{e}_{\text{old}}}{n} - \left(\cos\beta - \frac{\cos\alpha}{n}\right)\cdot \underline{N}, \tag{5}$$

where α and β are the angles of incidence and refraction, respectively, and $n = n_{\text{new}}/n_{\text{old}}$ is the relative refractive index (Fig. 2): if $n_{\text{old}} = n_0$, then $n_{\text{new}} = n_1$, and if $n_{\text{old}} = n_1$, then $n_{\text{new}} = n_2$.

3. Light Intensity Distribution below the Lens

We studied the path of light rays propagating through the lens, the refractive surfaces of which are described by the functions $f_1(r), f_2(r), f_3(r), f_4(r)$, and $f_5(r)$ in Eq. (1) (Fig. 1). Since the trilobite lens is rotationally symmetric, these five functions are rotated around the z axis, resulting in the 3D model of the lens. Consider a trilobite lens illuminated by a homogeneous light beam parallel to the optical axis. Let the cross section of the beam be a circle. Since in this case both the lens and the ray path are rotationally symmetric, this 3D optical problem can be transformed to a two-dimensional (2D) problem with the following trick: Let the cross-section of the homogeneous light beam be divided into m zones (e.g., $m = 10$ in Fig. 3). Zone $k = 1$ is circular in the center around the optical axis with radius r, while zones $1 < k \le m$ are rings, the width of which is r:

$$r = R/m, \tag{6}$$

where R is the lens radius, and $r = \text{square root}\,(x^2 + y^2)$. The area of the kth zone is

$$A_k = (kr)^2\pi - [(k-1)r]^2\pi = (2k-1)r^2\pi = (2k-1)R^2\pi/m^2,\quad k = 1, 2, \ldots, m. \tag{7}$$

The cross section of the incoming homogenous light beam [Fig. 3(a)] is

$$A_{\text{beam}} = R^2\pi, \tag{8}$$

and the full power of the beam is

$$P_{\text{beam}} = I_{\text{beam}} \cdot A_{\text{beam}}, \tag{9}$$

where I_{beam} is the homogeneous light intensity. The power of light coming from the kth zone is

$$P_k = P_{\text{beam}} A_k / A_{\text{beam}} = I_{\text{beam}} A_k, \tag{10}$$

where A_k is the cross-sectional area of the kth zone. We computed the light intensity below the lens along the optical axis. We considered a cylinder with length $14R$ with radius $\rho = 0.002 \cdot R$ along the optical axis below the lens, and this cylinder was divided into small cylindrical cells with height 2ρ (Fig. 3(b)). This resulted in 3500 elementary cells along the optical axis below the lens. Each ray coming from an arbitrary elementary ring-shaped zone of the paraxial incoming beam intersects the optical axis at the same point, the position of

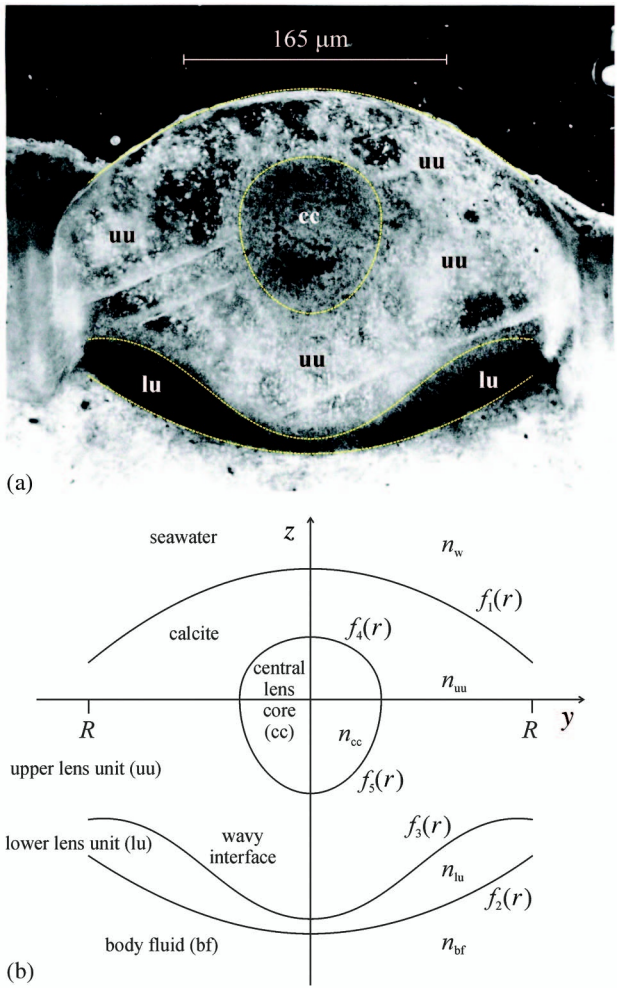

Fig. 1. (a) Main longitudinal section of the central-cored lens in a Silurian *Dalmanites* parallel to the optical axis of the lens (after Fig. 3 on p. 664 in [15]). Cc, central core; uu, upper unit; lu, lower unit. (b) Shape of the refractive surfaces of the *Dalmanites* lens in the coordinate system. $f_1(r)$, outer lens surface; $f_2(r)$, inner lens surface; $f_3(r)$, interface between the upper and lower lens units; $f_4(r)$, upper surface of the core; $f_5(r)$, lower surface of the core; R, lens radius; n_w, refractive index of seawater; n_{uu}, refractive index of the upper lens unit; n_{lu}, refractive index of the lower lens unit; n_{cc}, refractive index of the central core; n_{bf}, refractive index of body fluid; Z, optical axis of the lens coinciding with the axis of rotation symmetry.

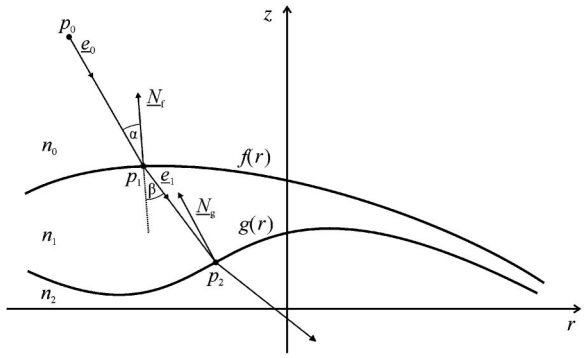

Fig. 2. Path of a light ray starting from point p_0 with direction $\underline{e}_0$, if there are two refracting surfaces, the vertical main longitudinal sections of which are described by the functions $f(r)$ and $g(r)$. The refractive indices of the different optical media are n_0, n_1, and n_2. The direction of the refracted ray is $\underline{e}_1$ after refraction at point p_1. The angles of incidence and refraction are α and β, respectively. The normal vectors of the refractive surfaces $f(r)$ and $g(r)$ are $\underline{N}_f$ and $\underline{N}_g$ at points p_1 and p_2, respectively. $\underline{e}_0$, $\underline{e}_1$, $\underline{N}_f$, and $\underline{N}_g$ are unit vectors ($e_0 = e_1 = N_f = N_g = 1$).

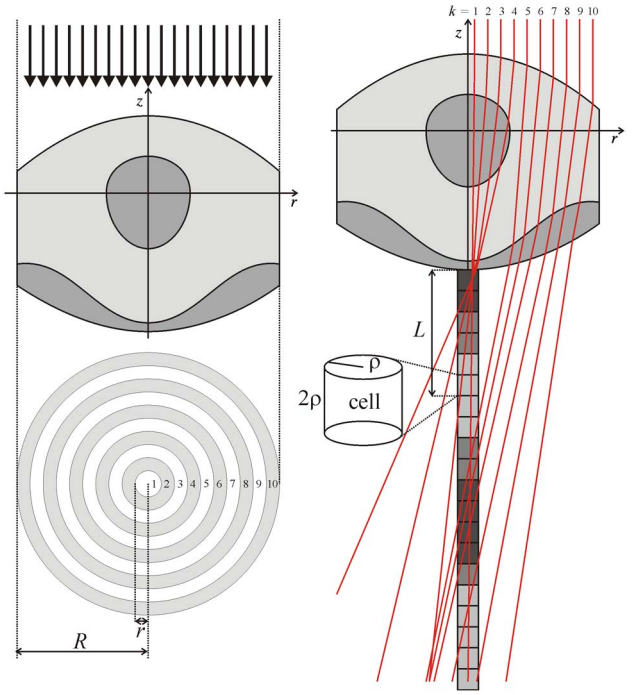

Fig. 3. (Color online) (a) Division of a paraxial homogenous light beam into $m = 10$ zones, for example. (b) Ray-tracing through the main longitudinal section of a central-cored trilobite lens to calculate the intensity along the optical axis below the lens. The darker the infinitesimal cylindrical cells (with radius ρ, and height 2ρ) along the optical axis, the more rays pass through them.

which was calculated with the use of ray-tracing described above. At the beginning of the computer modeling, the intensity value of each cell was set to zero. After this, $m = 500\,000$ rays parallel to the optical axis were incident on the lens. To kth ray belongs the kth ring of the incoming light beam. After refraction at the lens surfaces, the intersection of the optical axis and the ray exiting the lens was calculated, and the intensity value of the cell that was hit by a ray was increased by

$$\Delta I_k = P_k / A_{\text{cell}}, \qquad A_{\text{cell}} = \rho^2 \cdot \pi, \tag{11}$$

where A_{cell} is the cross section of the cell. From Eqs. (10) and (11) it follows that

$$\Delta I_k = (I_{\text{beam}} A_k)/(\rho^2 \pi). \tag{12}$$

After performing this procedure for all m rays, the series of cells [Fig. 3(b)] contains the values of the intensity I as a function of the distance L from the lowermost point of the lens along the optical axis below the lens [Fig. 3(b)]. In this work we display the relative intensity $i = I/I_{\text{beam}}$ versus the relative distance $l = L/R$. Function $i(l)$ was studied versus the refractive index n_{lu} of the lower lens unit and the refractive index n_{cc} of the central core with a resolution of $\Delta n_{\text{lu}} = \Delta n_{\text{cc}} = 0.0025$ in the following ranges:

$$1.36 < n_{\text{lu}} < 1.68, \qquad 1.52 < n_{\text{cc}} < 1.74. \tag{13}$$

Although these ranges are slightly arbitrary, the reasoning behind why these ranges were chosen was the following: The refractive index of the possibly organic material of the lower lens unit could not be smaller than that of body fluid (1.36) and could not be very much larger than that of calcite (1.66). On the other hand, the refractive index of the central core could not be much smaller than that of dry chitin (1.56) and could not reach that of guanine (1.80). Different values of n_{lu} and n_{cc} result in different $i(l)$ curves with one [Fig. 4(a)], two [Fig. 4(b)], or three [Fig. 4(c)] relative intensity peaks. Thus, the central-cored trilobite lens can be monofocal [Fig. 4(a)], bifocal [Fig. 4(b)], or trifocal [Fig. 4(c)], depending on the refractive indices. Each curve $i(l)$ was smoothed by a Gaussian function; that is, the following convolution integral was calculated:

$$i(l)_{\text{smoothed}} = \int_{k=-\alpha}^{\alpha} i(k) \cdot \frac{1}{\sqrt{2\pi\sigma^2}} e^{-\frac{(l-k)^2}{2\sigma^2}} \mathrm{d}k$$
$$\text{with} \quad \sigma = 0.02 \cdot R\,(= \text{length of 10 cells}) \text{ and } \alpha = 5 \cdot \sigma. \tag{14}$$

In the relative intensity curve $i(l)$, each peak and its immediate surrounding represents a focal point and a focal region, respectively. We define the sharpness

$$Q = h/w \tag{15}$$

of a focal point, where h is the height and w is the width of the peak at $i = 0.8 \cdot h$ [see inset in Fig. 4(a)]. In this work we consider Q as a quantitative measure of the correction for spherical aberration of a focal point. The reason for choosing a rather arbitrary value of 80% of the peak-value for the width is that if we chose much lower values (e.g., 50%), then it would be impossible to recognize separately two wide peaks being close to each other [e.g., Fig. 4(c)]. Hence, large h and small w result in a great Q-value. Peaks were detected looking for the satisfaction of the following two conditions:

1. $i(l_{i-1}) < i(l_i)$ and $i(l_{i+1}) < i(l_i)$,

2. $Q \geq 4000$.

According to our experience, a threshold-value of $Q* = 4000$ was appropriate to detect all intensity peaks. Of course, the shape of the $i(l)$ curve also depends on the value of m. Too small an m-value results in false curves. Studying the shape of $i(l)$ versus m, we experienced that if $m < 10^3$, the shape of $i(l)$ depends strongly on m, while if $m > 10^5$, the curve of $i(l)$ converges to the real curve.

4. Comparison of the Results of True and Semi-3D Ray-Tracings

To make sure that our self-developed semi-3D ray-tracing program works correctly, we also computed the intensity distribution below the lens along the optical axis in true three dimensions. The method of ray-tracing in 3D is practically the same as in 2D, but all vectors must be 3D, and functions $f_1(x, y), \ldots, f_1(x, y)$, describing the refractive surfaces of the trilobite lens, must posses two variables (x and y). The method of true 3D ray-tracing used in this work was the same as used in our earlier work [30], in which we computed the distribution of light intensity below a sunlit water droplet.

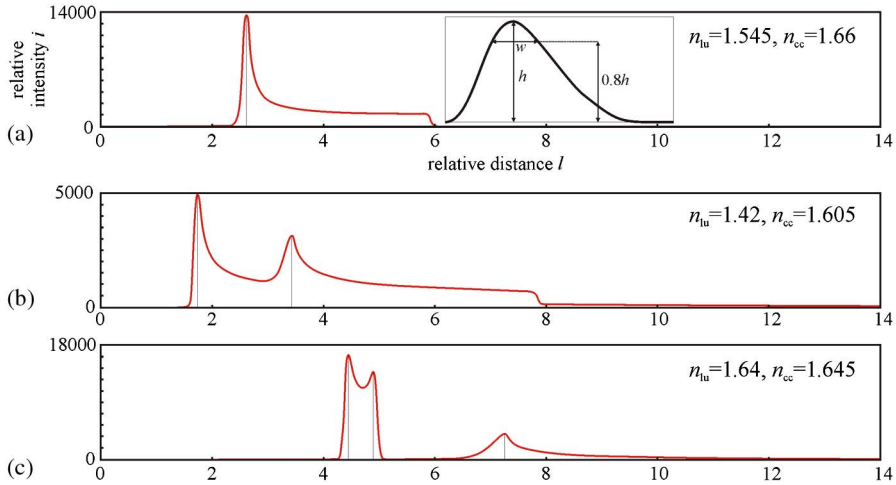

Fig. 4. (Color online) Examples for the relative intensity $i = I/I_{\text{beam}}$ as a function of the relative distance $l = L/R$ from the bottom of the studied central-cored trilobite lens (Fig. 1). (a) One relative intensity peak, $n_{\text{lu}} = 1.545$, $n_{\text{cc}} = 1.66$. (b) Two peaks, $n_{\text{lu}} = 1.42$, $n_{\text{cc}} = 1.605$. (c) Three peaks, $n_{\text{lu}} = 1.64$, $n_{\text{cc}} = 1.645$. The inset in (a) defines the sharpness $Q = h/w$ of a focal point, where h is the height and w is the width of the peak at $i = 0.8 \cdot h$.

In the true 3D ray-tracing, we defined a matrix composed of 600×4000 elements below the central-cored trilobite lens in the x–z plane (Fig. 5). The value of the elements was initially set to zero. For every ray, the path through the lens was computed with the use of the Snellius–DesCartes law of refraction. After a given ray exited the lowermost lens surface, the matrix elements hit by this ray below the lens were increased by 1. This procedure was performed for all the $4 \cdot 10^6$ rays originating from a square (2000×2000) region above the lens and incident parallel to the optical axis. At the end of this

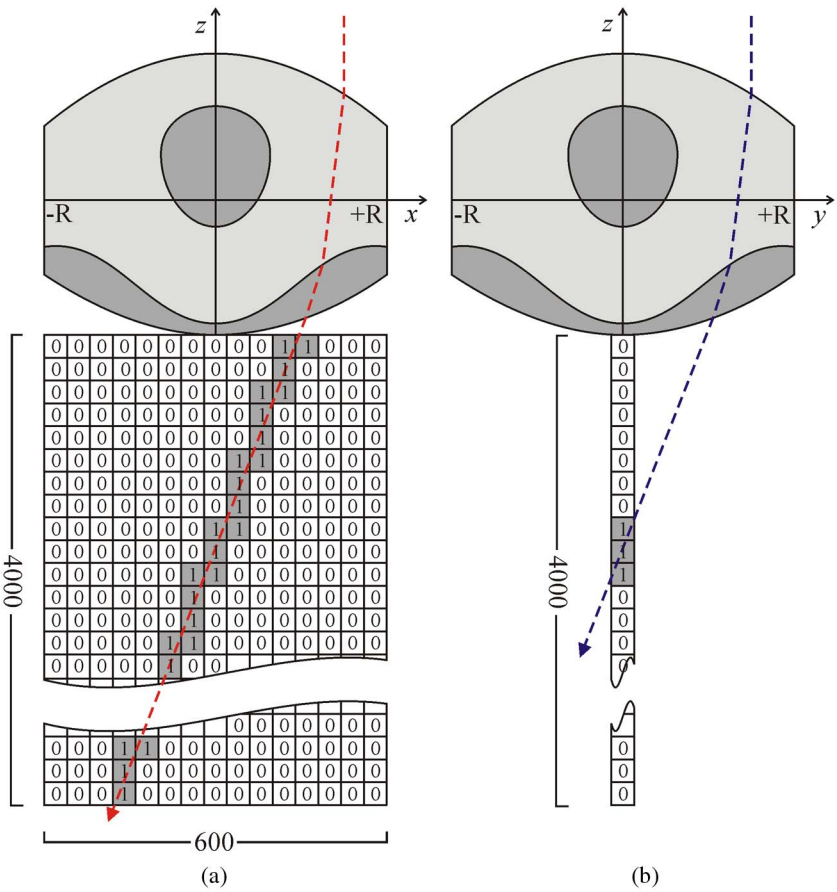

Fig. 5. (Color online) Computation of the intensity distribution below a central-cored trilobite lens in the x–z plane divided into 600×4000 cells representing a matrix, the elements of which were initially set to 0. The elements hit by a ray refracted by the lens are increased by 1. As examples, two rays [(a), red; (b), blue] are here shown starting from the point $\underline{p}_{\text{red}} = (0.75R, 0, R)$ and $\underline{p}_{\text{blue}} = (0, 0.75R, R)$, respectively, where R is the lens radius.

ray-tracing, the matrix contained information about the main cross section of the rotational symmetric intensity distribution below the lens. The light intensity along the optical axis is contained by the 300th column of the matrix. As we experienced, this true 3D ray-tracing gave the same results as the semi-3D ray-tracing. Since the true 3D ray-tracing needs much more computation time, we used the semi-3D ray-tracing throughout this work.

3. RESULTS

Figure 6 shows the paths of paraxially incident light rays through the investigated central-cored trilobite lens (Fig. 1), and the relative intensity i as a function of the relative distance l from the bottom of the lens along its optical axis, when the curve $i(l)$ has only one pronounced peak for different values of the refractive indices n_{lu} and n_{cc} of the lower lens unit and the central core, respectively. Figure 7 displays the curves $i(l)$ and ray-tracings computed for different values of n_{lu} and n_{cc} when $i(l)$ has two pronounced peaks. Figure 8 presents the curves $i(l)$ and ray-tracings for different values of n_{lu} and n_{cc} when $i(l)$ has three pronounced peaks. In Fig. 7 it can be well seen that if the refractive index n_{cc} of the central core differs from that of the upper lens unit $n_{\mathrm{uu}} = 1.66 \neq n_{\mathrm{cc}}$, there are two focal areas: (i) one focal area is produced by the central lens region including the core and the central parts of both the upper and lower lens units, and (ii) the other focal area is due to the focusing of the peripheral lens region including the annular peripheral parts of both the upper and lower lens units. In this work we call the site a "focal point" where the relative intensity i of focused light is maximal. These two sites are actually not exact focal points, because the distribution of i of focused light around them is a more or less wide quasi-Gaussian function, rather than a Dirac delta function.

Figure 9 summarizes these results showing how the number (1, 2, 3) of peaks of $i(l)$ changes as functions of n_{lu} and n_{cc}. In Fig. 9 the red, green, and blue regions (see the online-only color version of this figure) represent the situations when the studied central-cored trilobite lens is monofocal [one peak in $i(l)$], bifocal [two peaks in $i(l)$], and trifocal [three peaks in $i(l)$].

In Fig. 9 the vertical and horizontal dashed lines represent $n_{\mathrm{lu}} = n_{\mathrm{cc}} = 1.66$, which is the refractive index (n_{uu}) of the upper lens unit composed of calcite. Thus, the horizontal dashed line with $n_{\mathrm{cc}} = 1.66$ corresponds to a trilobite lens without a central core, because in this case the refractive index of the core is equal to the surrounding upper lens unit. On the other hand, the vertical dashed line with $n_{\mathrm{lu}} = 1.66$ corresponds to a lens without a lower lens unit, because then the refractive index of the upper and lower units is equal. In Fig. 9 the region above this horizontal line ($n_{\mathrm{cc}} > n_{\mathrm{uu}} = 1.66$) represents a trilobite lens with a central core acting as a collecting (or positive, or convex) lens, since the refractive index of the core is greater than the surrounding calcite. Consequently, the focal length of the central lens region (where the core has an influence on the light rays passing through the lens) is closer to the lens than the focal length of the periphery of the lens (where the core has no effect on the light rays). Similarly, in Fig. 9, the region below the horizontal dashed line ($n_{\mathrm{cc}} < n_{\mathrm{uu}} = 1.66$) corresponds to a lens with a core acting as a diffuser (or negative, or concave) lens. In this case the central lens region with the core possesses a longer focal length than the periphery.

Moving along a horizontal line in Fig. 9 means that n_{lu} changes at a constant n_{cc}. For example, moving from point G_1 to B_3 through points G_2, G_3, G_4, G_5, G_6, B_1, B_2, and G_{13}, the focal region of the central lens region does not have any notable displacement or deformation. It stays in the vicinity of the bottom of the lens. However, the focal region of the periphery of the lens changes: at point G_1 the relative intensity i composed by the lens periphery has a definite peak at a relative distance $l \approx 1.4$, and decays to zero at $l \approx 9$. Passing through points G_2, G_3, G_4, G_5, and G_6, the i-peak moves away from the lens and the point of total decay moves closer to the lens. Between points G_6 and B_1, at the green-blue transition in Fig. 9, a third i-peak appears in the focal region of the lens periphery; thus the lens is trifocal here. A further increase of n_{lu} results in the two i-peaks of the lens periphery merging at G_{13}, meaning a bifocal trilobite lens. Increasing n_{lu} further, the single i-peak of the lens periphery splits into two peaks, meaning a trifocal lens.

Moving along a vertical line in Fig. 9 means that n_{cc} varies at a constant n_{lu}. For example, point R_{13} represents a lens with a diffusing central core. Since the curves $i(l)$ are studied here only for relative distances $l < 14$ from the lens, the i-peak of the central lens region is still not detected at R_{13}, because it is coming from the infinity while n_{cc} increases. The point where the i-peak of the central lens region can be detected is the red-green transition between points R_{13} and G_{33}. Thus, in Fig. 9 the oblique red–green border means that the focal region of the central core is exiting/entering our detection interval, but it still exists somewhere far away from the lens or even at the infinity. The same is true at the green-blue transition above points G_{21} and G_{20}, at the red-green transition above points R_{15} and R_{16}, and at the green-blue transition above point G_{19} being the continuation of the oblique red-green border. Above this border line there is a narrow elongated area colored blue in the green region of Fig. 9. In this narrow blue area the focal region of the central core approaches the furthest part of the decaying focal region of the lens periphery. While the i-peak of the core passes through this point, our algorithm detects three peaks, if the focal region of the core is not exactly at the point of the total decay of the focal region of the lens periphery, but is close to it. If the i-peak of the central core is practically at the same distance as the furthest point of the focal region of the lens periphery, only two i-peaks are detected at point G_{36} in Fig. 9. Increasing n_{cc} further, the core gradually disappears at point R_5, because its refractive index becomes equal to that of the surrounding calcite ($n_{\mathrm{uu}} = 1.66$). Moving upward in Fig. 9, the i-peak splits into two peaks, and passing from point G_{11} to G_5 the focal region of the central core moves closer and closer to the lens.

From Fig. 9 we can read the following additional information: (i) If $n_{\mathrm{cc}} < n_{\mathrm{uu}}$, the trilobite lens is bifocal, but the value of $\Delta n = n_{\mathrm{uu}} - n_{\mathrm{cc}}$ must be small enough (<0.1), because larger Δn differences would result in the central core scattering light, and thus would make the focal region of the core be far away, or be eliminated. (ii) If $n_{\mathrm{cc}} = n_{\mathrm{uu}}$, the lens is mainly monofocal with quite a sharp focal region, especially at point R_7 in Fig. 9. Only the interval $1.6000 < n_{\mathrm{lu}} < 1.6525$ is the exception, where the lens is bifocal. (iii) If $n_{\mathrm{cc}} > n_{\mathrm{uu}}$, the lens is bifocal.

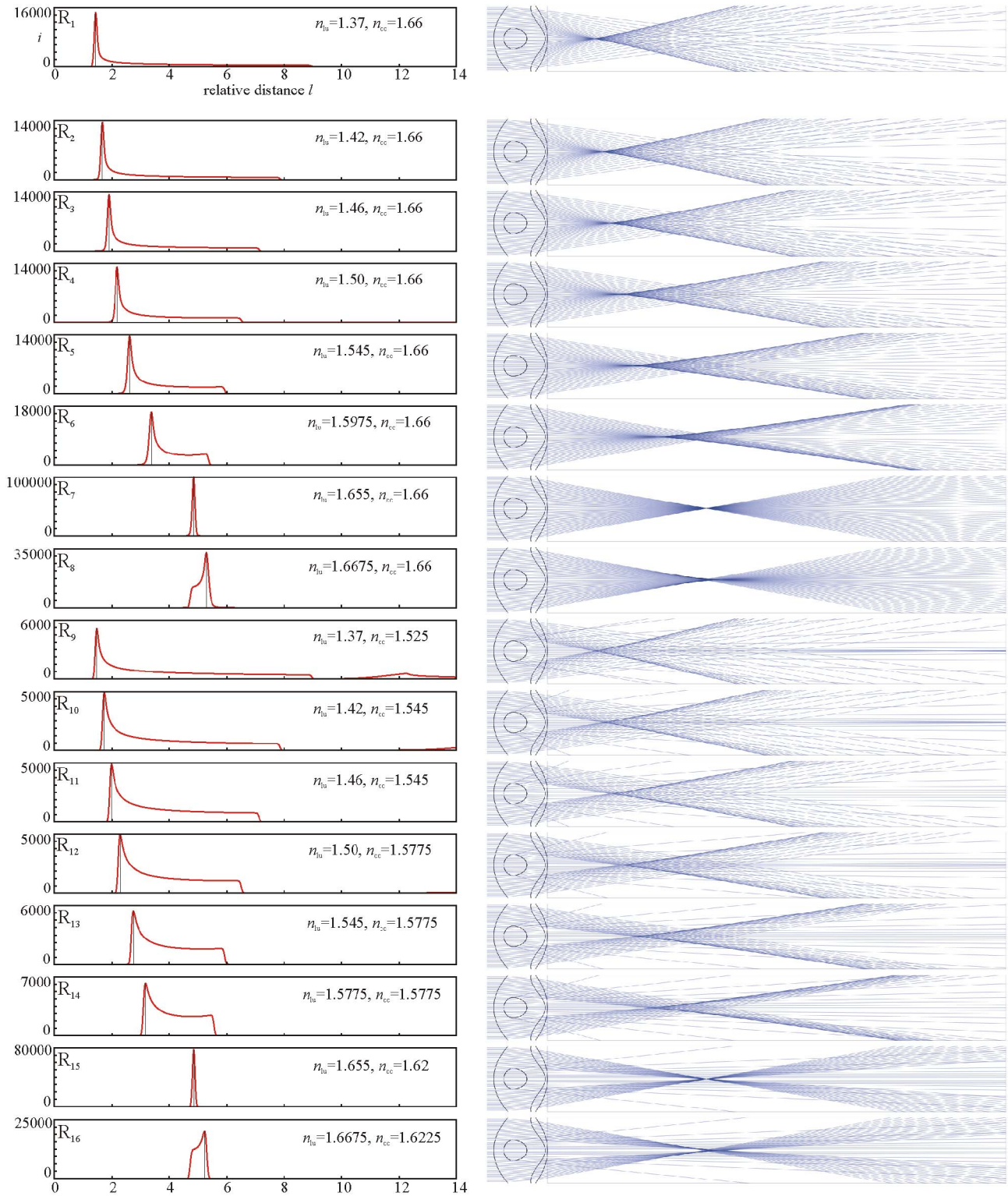

Fig. 6. (Color online) *Left*: relative intensity i as a function of the relative distance l from the bottom of the studied central-cored trilobite lens (Fig. 1) along the optical axis when the curve $i(l)$ has only one pronounced peak, the position of which is marked by a thin vertical line. The values of the refractive indices n_{lu} and n_{cc} of the lower lens unit and the central core, respectively, are given in the insets. The labels $R_1, \ldots, R_{16}$ correspond to the same labels in Fig. 9. *Right*: ray-tracing in the main longitudinal plane parallel to the optical axis of the lens.

Figure 10 shows the sharpness Q of a focal point as functions of the refractive indices n_{lu} and n_{cc} of the lower lens unit and the central core, if there is only a single $i(l)$-peak [Fig. 10(a)] and there are two $i(l)$-peaks [Figs. 10(b) and 10(c)]. The measure of correction for spherical aberration is Q; where Q is small or large, the lens is poorly or strongly corrected for spherical aberration, respectively. According to Fig. 10(a), in the case of monofocality, the parameter values

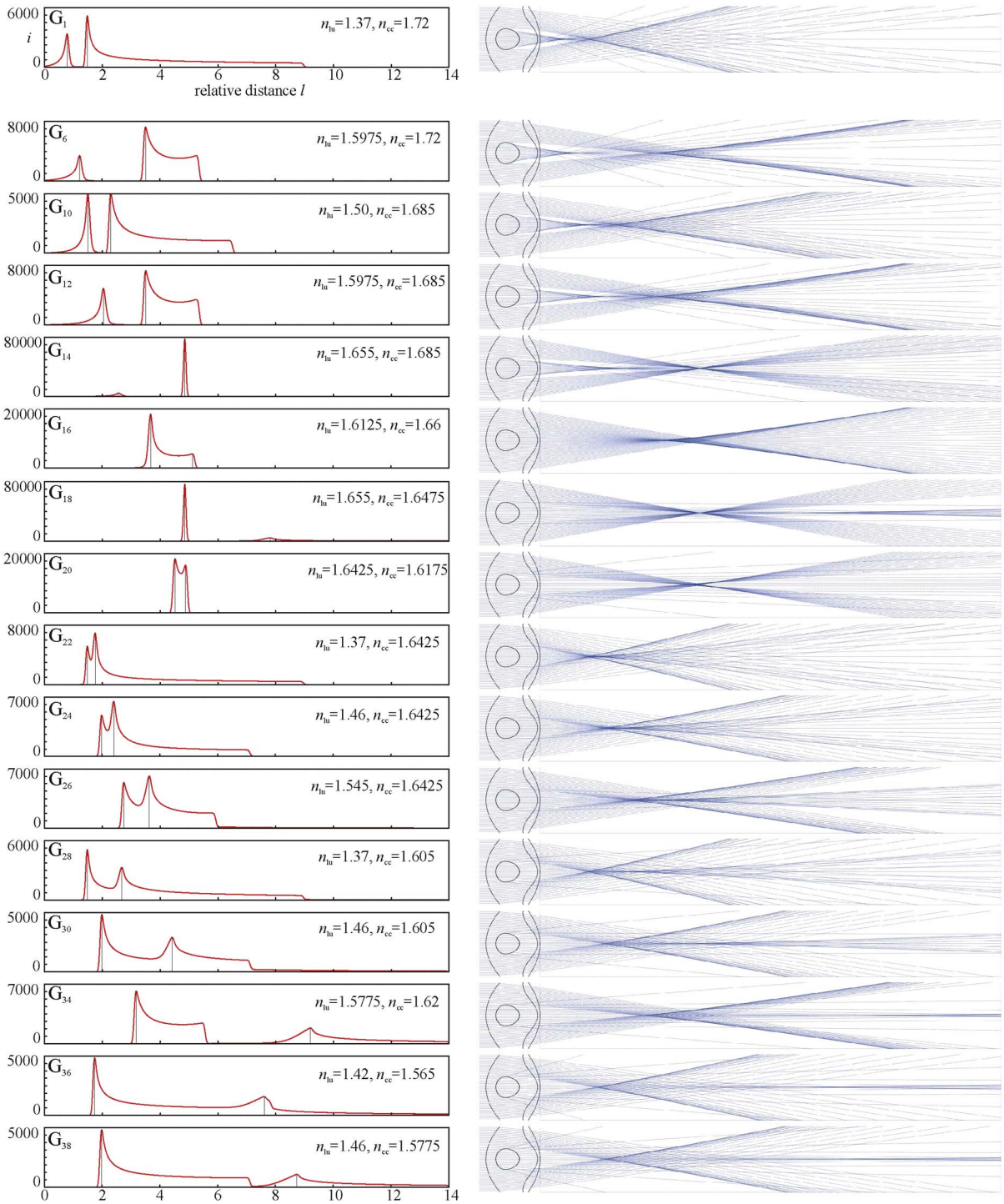

Fig. 7. (Color online) *Left*: Relative intensity i as a function of the relative distance l from the bottom of the studied central-cored trilobite lens (Fig. 1) along the optical axis when the curve $i(l)$ has two pronounced peaks, the positions of which are marked by thin vertical lines. The values of the refractive indices n_{lu} and n_{cc} of the lower lens unit and the central core, respectively, are given in the insets. The labels $G_1, \ldots, G_{38}$ correspond to the same labels in Fig. 9. *Right*: Ray-tracing in the main longitudinal plane parallel to the optical axis of the lens.

$n_{\mathrm{lu}} = 1.655$ and $n_{\mathrm{cc}} = 1.66$ give the highest Q. This means that there is no core and the lower lens unit has a slightly lower refractive index than the upper unit. In Fig. 10(b) we can see that the brightest area is just below the intersection of the horizontal and vertical dashed lines representing $n_{\mathrm{cc}} = 1.66$ and $n_{\mathrm{lu}} = 1.66$, but the same region is very dark in Fig. 10(c). From Fig. 10(c) it is clear that the highest Q-values are located just above the intersection of the mentioned two dashed lines, while in the same area in Fig. 10(b), Q is small. For a good bifocal lens, both focal points should have large and nearly equal Q-values. In the region above or below the line with $n_{\mathrm{cc}} = 1.66$ and smaller values of n_{lu} (e.g., 1.40), Q is almost the same for both focal points [Figs. 10(b) and 10(c)], meaning that both focal regions have nearly the same sharpness.

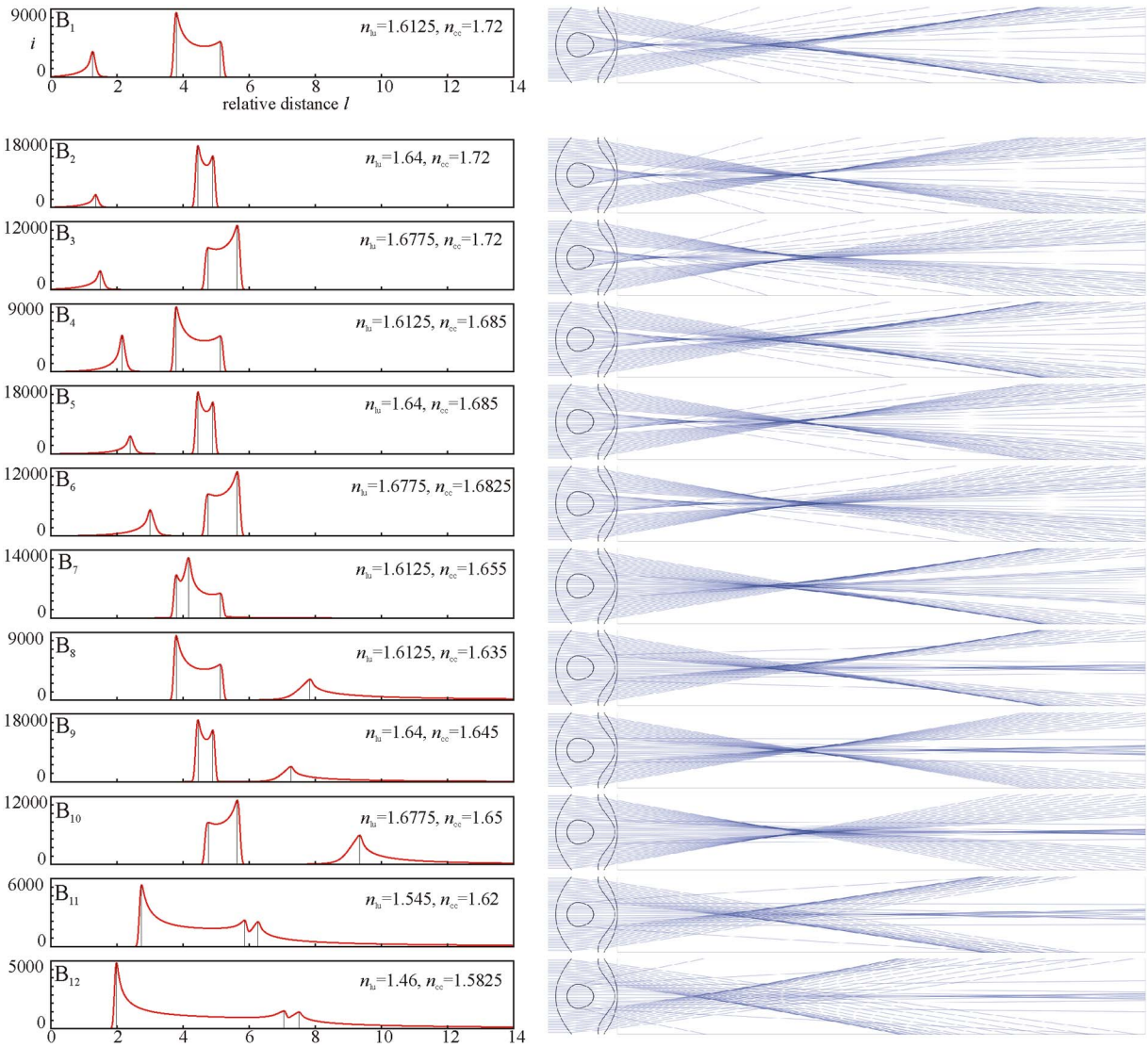

Fig. 8. (Color online) *Left*: relative intensity i as a function of the relative distance l from the bottom of the studied central-cored trilobite lens (Fig. 1) along the optical axis when the curve $i(l)$ has three pronounced peaks, the positions of which are marked by thin vertical lines. The values of the refractive indices n_{lu} and n_{cc} of the lower lens unit and the central core, respectively, are given in the insets. The labels $B_1, \ldots, B_{38}$ correspond to the same labels in Fig. 9. *Right*: ray-tracing in the main longitudinal plane parallel to the optical axis of the lens.

We performed the ray-tracing through the studied central-cored trilobite lens as a function of the angle of incidence θ of parallel rays for $n_{\mathrm{cc}} = 1.64$ and $n_{\mathrm{cc}} = n_{\mathrm{uu}} = 1.66$. In the latter case the upper lens unit is optically homogeneous; that is, there is no central core. It became clear from these computations that as θ increases, the bifocality of the lens gradually diminishes, because the off-axis rays cannot form sharp focal regions (points). The same was true for the monofocal lens without a central core. The off-axis ray-tracing through the doublet lens in the larvae of the leaf wasp *Perga* [24] was very similar to that in the studied central-cored trilobite lens.

4. DISCUSSION

To understand the possible optical function(s) of the central core of the lenses in the compound eyes of *Dalmanites* trilobites, we performed computational ray-tracing on such a lens, the refractive surfaces of which have been reconstructed earlier [15]. The upper lens unit of central-cored schizochroal trilobite lenses was composed of optically homogeneous calcite with a refractive index $n_{\mathrm{uu}} = 1.66$ [15]. Although the material composition of the central core and the lower lens unit is unknown, from their homogeneous appearance in optical and electron microscopic imaging it is assumed that they might have been homogeneous [3,5,8,9,22,31].

In the literature of trilobite vision (reviewed in [5,8,9,22,31]), it is generally accepted, as the simplest optical model, that the upper lens unit was composed of homogeneous calcite (which remained during fossilization, and thus it is known that its crystallographic c-axis was *in vivo* parallel to the optical axis of the lens, with a refractive index of 1.66.), and the lower lens unit was a homogeneous material composed of hydrated chitin or other organic material with a constant refractive index ranging between 1.4 and 1.53. Although the material composition of the central core is unknown, due to its homogeneous appearance in thin-sections it is logical to assume that it was also optically homogeneous. This work is the first attempt to understand the function of the central core, and it was logical to start with the simplest optical

model. Thus, the homogeneity of the lens units of central-cored trilobite lenses is a sound hypothesis.

On the other hand, due to the several-hundred-million-year fossilization, the material composition of the central core in trilobite lenses is unknown. The original core material has disappeared and been replaced by mineral materials during the long diagenesis. Only the shape of the central core could be reconstructed from thin sections of lenses [15]. The same is true for the lower lens unit. Consequently, the indices of refraction of the lower lens unit and the central core cannot be measured. The only thing we can do is consider an optical model of the central-cored trilobite lens and study it with computational ray-tracing. It was logical to consider first the simplest model: we assumed that all three lens units (upper unit, lower unit, central core) were optically homogeneous with constant refractive indices. We showed here that under certain conditions (parameter configurations of the refractive indices of the homogeneous lens units), the studied model lens could function as a spherically corrected monofocal, bifocal, or trifocal lens. The trifocal version was rejected as a visually nonfunctionable case, while the spherically corrected monofocal and bifocal versions were accepted as possible optically well-functioning lenses. Hence, the simplest assumption, i.e., the tripartite trilobite lens with homogeneous units, is optically/visually sound. If the result of the computational ray-tracing were that under the assumed conditions (homogeneous lens units) the tripartite lens could not function, then it would be worth studying another optical model of the trilobite lens. Such a model could be a tripartite lens with radial or horizontal gradients of refractive indices (both kinds of arrangement occur in the dioptric apparatuses of insects [32]). Studying this model could be an interesting task of future research.

We studied the relative intensity i of light focused by the lens versus the relative distance l from the lower lens surface along the optical axis as functions of the refractive indices n_{lu} and n_{cc} of the lower lens unit and the central core, respectively. We determined those values of n_{lu} and n_{cc} that ensure that the studied central-cored trilobite lens is monofocal, bifocal, or trifocal (Fig. 9). Both the structural and optical appearances of the core are obviously different from those of the upper lens unit [Fig. 1(a)], which hints at an optically different material resulting in a different index of refraction. The possibility that the core has not existed *in vivo*, but came into

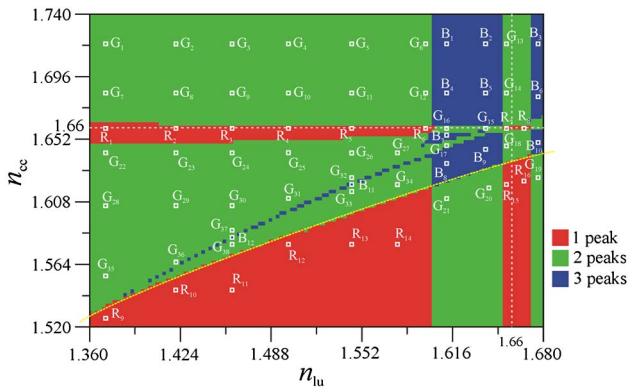

Fig. 9. (Color online) The sides of the large rectangle represent the intervals of the refractive indices n_{lu} and n_{cc} of the lower lens unit and the central core in the studied central-cored trilobite lens (Fig. 1). A given point in the rectangle corresponds to a given value-pair $(n_{\mathrm{lu}}, n_{\mathrm{cc}})$. The positions of the small white squares represent the values $(n_{\mathrm{lu}}, n_{\mathrm{cc}})$ for which the relative intensity i was computed versus the relative distance l from the bottom of the lens along its optical axis. The colors (red, green, blue) and labels (R, G, B) represent the number (1, 2, 3) of pronounced peaks of the curve $i(l)$, some of which are shown in Figs. 6, 7, and 8. The vertical and horizontal white dashed lines represent $n_{\mathrm{lu}} = n_{\mathrm{cc}} = 1.66$. The yellow dashed line represents the situations where the detection of the furthest focal point become possible: below this line the furthest focal point is out of view.

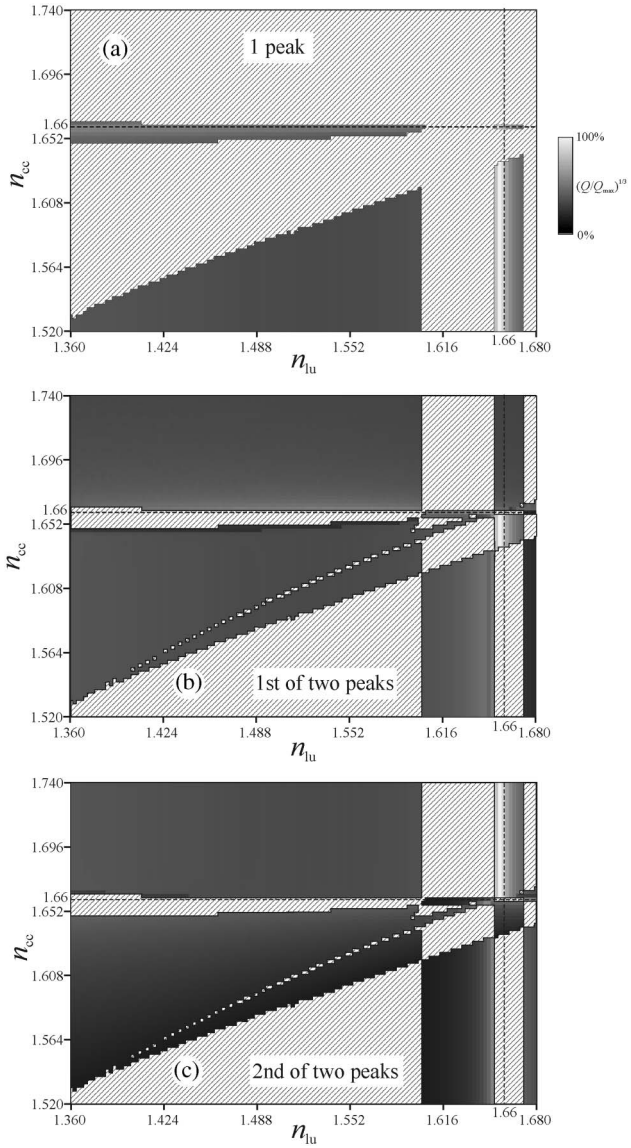

Fig. 10. Sharpness Q of a focal point [defined by Eq. (15) and Fig. 4(a)] as functions of the refractive indices n_{lu} and n_{cc} of the lower lens unit and the central core. (a) $Q(n_{\mathrm{lu}}, n_{\mathrm{cc}})$ of the single peak of $i(l)$ for values of $(n_{\mathrm{lu}}, n_{\mathrm{cc}})$ represented by red (medium gray in print) in Fig. 9. (b) $Q(n_{\mathrm{lu}}, n_{\mathrm{cc}})$ of the first (closer to the lens) peak of $i(l)$ for values of $(n_{\mathrm{lu}}, n_{\mathrm{cc}})$ represented by green (light gray in print) in Fig. 9. (c) $Q(n_{\mathrm{lu}}, n_{\mathrm{cc}})$ of the second (further from the lens) peak of $i(l)$ for values of $(n_{\mathrm{lu}}, n_{\mathrm{cc}})$ represented by green in Fig. 9. The darker the gray, the smaller the value of Q in such a way that the gray shades code the values of $q = (Q/Q_{\max})^{1/3}$, where $Q_{\max} = 3096223$ (black: $Q = 0$, $q = 0\%$; white: $Q = Q_{\max}$, $q = 100\%$). In diagram (a), those areas are striped where the numbers of $i(l)$-peaks are 2 or 3 (coinciding with the green and blue (dark, upper right in print) regions in Fig. 9). In diagrams (b) and (c), those areas are striped where the numbers of $i(l)$-peaks are 3 or 1 (coinciding with the blue and red regions in Fig. 9).

being during fossilization as a diagenetic artifact, has been excluded by earlier studies [12,15].

On the basis of the results presented here, one of the possible optical functions of the central core in the schizochroal eye of the investigated Silurian *Dalmanites* (Fig. 1) could have been correction for spherical aberration, independently of the number (1, 2, or 3) of focal points. During our computations, we experienced that the peaks of the relative intensity curves $i(l)$ are more or less pronounced (Figs. 4, 6, 7, and 8). The sharpness Q of these peaks is defined by Eq. (15).

For the values of n_{lu} and n_{cc} represented by green color in Fig. 9, the investigated central-cored trilobite lens (Fig. 1) is bifocal. Thus, another possible optical function of the core could have been to ensure bifocality of the lens. In this case the peripheral lens region could have a given focal length and the central lens region could possess a longer or shorter focal length, if the refractive index n_{cc} of the core was smaller or larger than the refractive index n_{lu} of the upper lens unit. The refractive index of the calcite upper lens unit was 1.66, which is a very high value, much higher than the refractive index of organic materials, such as chitin, for example, with $n_{\mathrm{chitin}} \approx$ 1.45–1.56, depending on the state of hydration of chitin [33,34]. In our opinion, it is improbable that the refractive index of the core was larger than that of calcite. If n_{cc} was smaller than that of the upper lens unit, the core ensured a longer focal length centrally than the shorter focal length of the peripheral lens region (Fig. 7). The larger the refractive index difference between the core and the upper unit, the greater the difference between the central and peripheral focal lengths.

The optical sense of bifocality of lenses can be the following: Gál *et al.* [19,29] discovered two cases for bifocality among trilobite lenses. They showed [19] that the bifocal lenses of the schizochroal-eyed trilobite *Dalmanitina socialis* could have enabled the trilobite to see simultaneously both very near (e.g., floating food particles and tiny prey) and far (e.g., sea floor, conspecifics, or approaching enemies) in the optical environment through the central and peripheral lens regions, respectively, if the retina was placed at the focal point further away from the lens (produced by the peripheral lens region). In *Dalmanitina socialis* the lower surface of the upper calcite lens unit possessed a central bulge with a high curvature ensuring a higher refractive power, and thus resulting in a shorter central focal length than the longer focal length of the peripheral lens region.

From the results presented in [19] it follows that if the retina of the Silurian *Dalmanites* trilobite studied in this work was at the central focal point (being farther away from the lens and produced by the central lens region), the trilobite could have seen simultaneously both near and far through its peripheral and central lens regions, respectively. Hence, in *Dalmanites* the functions of the central and peripheral lens regions (seeing near/far through the peripheral/central lens region) could have been the reverse of those in *Dalmanitina socialis* (seeing near/far through the central/peripheral lens region).

More than two focal points of lenses in compound eyes would be too many, and the image forming of such lenses would be too complex. Furthermore, the principal image formed by such lenses on the retina would be blurred by the multiple (secondary and tertiary) images being out of focus. Consequently, the trifocality of the studied central-cored trilobite lens (Fig. 1), represented by blue color in Fig. 9, can be considered only as a theoretical option, but by no means an optically optimally functioning possibility. Thus, in our opinion, the use of trifocal lenses in trilobite eyes was out of the question.

REFERENCES

1. H. B. Whittington, *Fossils Illustrated 2—Trilobites* (Boydell, 1992).
2. K. M. Towe, "Trilobite eyes: calcified lenses in vivo," Science **179**, 1007–1009 (1973).
3. E. N. K. Clarkson, "The visual system of trilobites," Palaeontology **22**, 1–22 (1979).
4. E. N. K. Clarkson, "The eye, morphology, function and evolution," in *Treatise on Invertebrate Paleontology, part O, Trilobita, Revised*, R. L. Kaesler et al., eds. (University of Kansas, 1997), pp. 114–132.
5. R. Levi-Setti, *Trilobites*, 2nd ed. (University of Chicago, 1993).
6. A. T. Thomas, "Developmental palaeobiology of trilobite eyes and its evolutionary significance," Earth Sci. Rev. **71**, 77–93 (2005).
7. E. N. K. Clarkson, "The evolution of the eye in trilobites," Fossils Strata **4**, 7–31 (1975).
8. R. Levi-Setti, E. N. K. Clarkson, and G. Horváth, "Paleontologia dell'occhio (Paleontology of the eye)," in *Frontiere della Vita—Enciclopedia Italiana (Frontiers of Biology—Italian Encyclopedia). I. Origine ed evoluzione della vita. (Origin and Evolution of Life) 7. La construzione degli organismi (Construction of the Organism)*, D. Baltimore, R. Dulbecco, F. Jacob, and R. Levi-Montalcini, eds. (1998), pp. 365–379 (in Italian). http://www.treccani.it
9. R. Levi-Setti, E. N. K. Clarkson, and G. Horváth, "The eye: paleontology," in *Frontiers of Biology—Italian Encyclopedia. Part I. Origin and Evolution of Life. Section 7. Construction of the Organism*, D. Baltimore, R. Dulbecco, F. Jacob, and R. Levi-Montalcini, eds. (2002), pp. 379–395.
10. R. A. Fortey, "Pelagic trilobites as an example of deducing the life habits of extinct arthropods," Trans. R. Soc. Edinburgh Earth Sci. **76**, 219–230 (1985).
11. T. McCormick and R. A. Fortey, "Independent testing of a paleobiological hypothesis: the optical design of two pelagic trilobites reveals their relative palaeobathymetry," Paleobiology **24**, 235–253 (1998).
12. J. Miller and E. N. K. Clarkson, "The post-ecdysial development of the cuticle and the eye of Phacops rana milleri," Philos. Trans. R. Soc. Lond. Ser. B **288**, 461–480 (1980).
13. E. N. K. Clarkson, "Fine structure of the eye in two species of Phacops (Trilobita)," Palaeontology **10**, 603–616 (1967).
14. G. Lindström, "Researches on the visual organs of the trilobites," Kongliga Svenska Vertenskaps Akademiens Handlingar **8**, 1–89 (1901).
15. E. N. K. Clarkson and R. Levi-Setti, "Trilobite eyes and the optics of Des Cartes and Huygens," Nature **254**, 663–667 (1975).
16. G. Horváth, "Geometric optics of trilobite eyes: a theoretical study of the shape of aspherical interface in the cornea of schizochroal eyes of phacopid trilobites," Math. Biosci. **96**, 79–94 (1989).
17. G. Horváth and E. N. K. Clarkson, "Computational reconstruction of the probable change of form of the corneal lens and maturation of optics in the post-ecdysial development of the schizochroal eye of the Devonian trilobite Phacops rana milleri Stewart 1927," J. Theor. Biol. **160**, 343–373 (1993).
18. G. Horváth, "The lower lens unit in schizochroal trilobite eyes reduces reflectivity: on the possible optical function of the intralensar bowl," Hist. Biol. **12**, 83–92 (1996).
19. J. Gál, G. Horváth, E. N. K. Clarkson, and O. Haiman, "Image formation by bifocal lenses in a trilobite eye?" Vis. Res. **40**, 843–853 (2000).
20. M. Lee, C. Torney, and A. W. Owen, "Magnesium-rich intralensar structures in schizohroal trilobite eyes," Palaeontology **50**, 1031–1038 (2007).
21. R. Feist, "The effect of paedomorphosis in eye reduction on patterns of evolution and extinction in trilobites," in *Evolutionary*

Change and Heterochrony, K. J. McNamara, ed. (Wiley, 1995), pp. 225–244.
22. E. Clarkson, R. Levi-Setti, and G. Horváth, "The eyes of trilobites: the oldest preserved visual system," Arthropod Struct. Dev. **35**, 247–259 (2006).
23. G. Horváth, E. N. K. Clarkson, and W. Pix, "Survey of modern counterparts of schizochroal trilobite eyes: structural and functional similarities and differences," Hist. Biol. **12**, 229–263 (1997).
24. V. B. Meyer-Rochow, "Structure and function of the larval eye of the sawfly, Perga," J. Insect Physiol. **20**, 1565–1591 (1974).
25. E. Buschbeck, B. Ehmer, and R. Hoy, "Chunk versus point sampling: visual imaging in a small insect," Science **286**, 1178–1180 (1999).
26. D. Fordyce and T. W. Cronin, "Trilobite vision: a comparion of schizochroal and holochroal eyes with compound eyes of modern arthropods," Paleobiology **19**, 288–303 (1993).
27. B. Schoenemann, "Trilobite eyes and a new type of neural superposition eye in an ancient system," Palaeontographica A **281**, 63–91 (2007).
28. X. G. Zhang and E. N. K. Clarkson, "The eyes of Lower Cambrian eodiscid trilobites," Palaeontology **33**, 911–933 (1990).
29. J. Gál, G. Horváth, and E. N. K. Clarkson, "Reconstruction of the shape and optics of the lenses in the abathochroal-eyed trilobite Neocobboldia chinlinica," Hist. Biol. **14**, 193–204 (2000).
30. Á. Egri, Á. Horváth, G. Kriska, and G. Horváth, "Optics of sunlit water drops on leaves: conditions under which sunburn is possible," New Phytologist **185**, 979–987 (2010).
31. E. N. K. Clarkson, R. Levi-Setti, and G. Horváth, "The eyes of trilobites: the oldest preserved visual system + Los ojos de los trilobites: el sistema visual más antiguo conservado (in Spanish)," Fundam. Appl. Nematol. **13**, 1–70 (2008).
32. M. F. Land and D.-E. Nilsson, *Animal Eyes* (Oxford University, 2002), p. 221.
33. H. Hinton and G. Jarman, "Physiological colour change in the Hercules beetle," Nature **238**, 160–161 (1972).
34. M. F. Land, "The physics and biology of animal reflectors," Prog. Biophys. Mol. Biol. **24**, 75–106 (1972).